Langmuir **2007,** *23,* 265−273

Adaptive Nanomechanical Response of Stratified Polymer Brush Structures[†]

M. C. LeMieux,[‡] S. Peleshanko,[‡,§] K. D. Anderson,[‡] and V. V. Tsukruk*[,‡,§]

Department of Materials Science and Engineering, Iowa State University, Ames, Iowa 50011, and
School of Materials Science and Engineering, Georgia Institute of Technology, Atlanta, Georgia 30332

Received June 15, 2006. In Final Form: September 10, 2006

We have fabricated a stratified polymer surface film with tunable thickness (within 17−34 nm) through facile, room-temperature, UV-initiated polymerization with a temperature-sensitive pNIPAAM layer confined beneath a hydrophobic layer. AFM morphology and ellipsometric measurements were measured at each grafting step, along with XPS measurements of the overall layer to verify layer growth. The strong characteristic LCST behavior of pNIPAAM was observed in water, with a 100% change in thickness above and below this transition. The AFM nanomechanical results demonstrate vertical gradients of the elastic response tunable to a desired state by the external temperature. These temperature-sensitive, adaptive polymer structures with the pNIPAAM layer "hidden" beneath the rubbery, hydrophobic PBA topmost layer represent an interesting example of nanoengineering surfaces with properties such as adhesion, elastic modulus, and multi-level structural reorganization responsive to fluidic and temperature variations that can be important for biological purposes such as implant coatings, cell-surface mimicry, and drug delivery vehicles.

Introduction

Highly complex biomaterials research is currently a very intense field requiring polymer scientists to develop synthetic replicas to mimic biological internal structures. Nearly all important biological structures have evolved through a bottom-up "synthesis" in which the final nanoscaffolds have a common feature of possessing a hierarchal structure with each level performing a separate, different function.[1,2] Engineering new polymer surfaces involves designing complex architectures with features such as graded branching and composition that will lead to novel material properties in terms of mechanical behavior, adaptability, and functionality. Polymer brushes, which possess an intrinsic remarkable stimuli-responsive nature, represent one area of intense research in polymer science regarding adaptive surfaces.[3,4] Another area that will be key for expanding the nanotechnology frontier from the polymer science aspect is macromolecular architecture engineering.[5−8] The combination of the two will lead to new surfaces that are imperative for the next generation of nanoscale devices with novel conformations (confinements) inducing secondary intramolecular interactions leading to unusual nanomechanical and nanotribological properties.[9−16]

Nanoscale devices and their operating environments require adaptive surfaces constructed with smart properties that can not only sense or respond to environmental stimuli but can also be robust and possess tailored, on-demand physical properties.[17−20] Thus, polymer surface modification, which inherently provides the ability to control and change surface composition, allowing on-demand properties, is becoming increasingly significant for practical applications in fields such as nanoscale lubrication, sensing, and biocompatibility[21−28] or the exciting advancement of functional carbon nanotube devices.[29−32] Polymer brush layers are considered to be ideal choices in such applications for several

---

[†] Part of the Stimuli-Responsive Materials: Polymers, Colloids, and Multicomponent Systems special issue.

[*] To whom correspondence should be addressed. E-mail: vladimir@mse.gatech.edu.

[‡] Iowa State University.

[§] Georgia Institute of Technology.

(1) Tomalia, D. A.; Mardel, K.; Henderson, S. A.; Holan, G.; Esfand, R. In *Handbook of Nanoscience, Engineering, and Technology*; Goddard, W. A., III et al., Eds.; CRC Press: Boca Raton, FL, 2003; pp 1−34.

(2) Goodsell, D. S. *Am. Sci.* **2000**, *88*, 230.

(3) Luzinov, I.; Minko, S.; Tsukruk, V. V. *Prog. Polym. Sci.* **2004**, *29*, 635. Zhao, B.; Brittain, W. J. *Prog. Polym. Sci.* **2000**, *25*, 677.

(4) Advincula, R. C.; Brittain, W. J.; Caster, K. C.; Ruhe, J. *Polymer Brushes*; Wiley: Weinheim, Germany, 2004.

(5) Matyjaszewski, K. *Prog. Polym. Sci.* **2005**, *30*, 858.

(6) Frauenrath, H. *Prog. Polym. Sci.* **2005**, *30*, 325.

(7) Hadjichristidis, N.; Pitsikalis, M.; Iatrou, H.; Pispas, S. *Macromol. Rapid Commun.* **2003**, *24*, 979.

(8) Nakayama, Y.; Sudo, M.; Uchida, K.; Matsuda, T. *Langmuir* **2002**, *18*, 2601.

(9) Tsukruk, V. V. *Adv. Mater.* **2001**, *13*, 95.

(10) Romiszowski, P.; Sikorski, A. *J. Chem. Inf. Comput. Sci.* **2004**, *44*, 393.

(11) Percec, V.; Ahn, C. H.; Ungar, G.; Yeardley, D. J. P.; Möller, M.; Sheiko, S. S. *Nature* **1998**, *391*, 161.

(12) Pakula, T.; Minkin, P.; Matyjaszweski, K. *ACS Symp. Ser.* **2003**, *854*, 366.

(13) Tian, P.; Uhrig, D.; Mays, J. W.; Watanabe, H.; Kilbey, S. M. *Macromolecules* **2005**, *38*, 2524.

(14) Ye, M.; Zhang, D.; Han, L.; Tejada, J.; Ortiz, C. *Soft Matter* **2006**, *2*, 243.

(15) Zhang, D.; Ortiz, C. *Macromolecules* **2005**, *38*, 2535.

(16) Zhang, D.; Ortiz, C. *Macromolecules* **2004**, *37*, 4271.

(17) Muller, R. S. In *Micro/Nanotribology and Its Applications*; Bhushan, B., Ed.; Kluwer Academic Press: Dordecht, The Netherlands, 1997; p 579. *Tribology Issues and Opportunities in MEMS*; Bhushan, B., Ed.; Kluwer Academic Publishers: Dordrecht, The Netherlands, 1997. Tsukruk, V. V. In *Nanotribology*; Hsu, S. M., Ying, C. Z., Eds.; Kluwer Academic Press: Boston, 2002; p 347.

(18) Santer, S.; Kopyshev, A.; Donges, J.; Yang, H.-K.; Rühe, J. *Macromolecules* **2006**, *22*, 4660. Genson, K. L.; Holzmuller, J.; Villacencio, O. F.; McGrath, D. V.; Vaknin, D.; Tsukruk, V. V. *J. Phys. Chem. B* **2005**, *109*, 20393. Julthongpiput, D.; Lin, Y. H.; Teng, J.; Zubarev, E. R.; Tsukruk, V. V. *Langmuir* **2003**, *19*, 7832. Julthongpiput, D.; Lin, Y.-H.; Teng, J.; Zubarev, E. R.; Tsukruk, V. V. *J. Am. Chem. Soc.* **2003**, *125*, 15912. Lin, Y.-H.; Teng, J.; Zubarev, E. R.; Shulha, H.; Tsukruk, V. V. *Nano Lett.* **2005**, *5*, 491. Xu, C.; Fu, X.; Fryd, M.; Xu, S.; Wayland, B. B.; Winey, K. I.; Composto, R. J. *Nano Lett.* **2006**, *6*, 282. Gunawidjaja, R.; Peleshanko, S.; Tsukruk, V. V. *Macromolecules* **2005**, *38*, 8765.

(19) Lemieux, M.; Usov, D.; Minko, S.; Stamm, M.; Shulha, H.; Tsukruk, V. V. *Macromolecules* **2003**, *36*, 7244.

(20) Tsukruk, V. V.; Luzinov, I.; Larson, K.; Li, S.; McGrath, D. V. *J. Mater. Sci. Lett.* **2001**, *20*, 873. Sidorenko, A.; Minko, S.; Schenk-Meuser, K.; Duschner, H.; Stamm, M. *Langmuir* **1999**, *15*, 8349. Peleshanko, S.; Sidorenko, A.; Larson, K.; Villavicencio, O.; Ornatska, M.; McGrath, D. V.; Tsukruk, V. V. *Thin Solid Films* **2002**, *406*, 233. Sidorenko, A.; Houphouet-Boigny, C.; Villavicencio, O.; McGrath, D. V.; Tsukruk, V. V. *Thin Solid Films* **2002**, *410*, 147. Larson, K.; Vaknin, D.; Villavicencrio, O.; McGrath, D. V.; Tsukruk, V. V. *J. Phys. Chem. B* **2002**, *106*, 7246. Genson, K. L.; Vankin, D.; Villavicencio, O.; McGrath, D. V.; Tsukruk, V. V. *J. Phys. Chem. B* **2002**, *106*, 11277.

(21) Ionov, L.; Minko, S.; Stamm, M.; Gohy, J.-F.; Jérôme, R.; Scholl, A. *J. Am. Chem. Soc.* **2003**, *125*, 8302. Liu, Y.; Klep, V.; Zdyrko, B.; Luzinov, I. *Langmuir* **2005**, *21*, 11806.

10.1021/la061723k CCC: $37.00

reasons. They are chemically tethered to the surface at one end, virtually any chemistry can be designed into the layer depending on intended surface interactions, and the high grafting density combined with uniformity in composition, thickness, and structure allows the entire surface to respond to local environmental stimuli.[3,9,33−38]

However, it is recognized that the stretched conformation of brush chains due to overlapping is the origin of intrinsic properties such as high compression resistance and excellent mechanical response.[35,39−41] Grafted multicomponent (mixed) brush layers allow for supreme interfacial manipulation.[42] Polymer brush layers with vertically graded branching/properties normal to the surface would be an ideal candidate in both cases. Rather than grafting two homopolymer brushes to create a mixed binary brush, an alternative route to responsive surfaces is grafting block copolymers of two chemically different blocks. These systems are attractive because of the very rich and interesting surface morphologies that are possible depending on block length ratios and interactions between the two blocks relative to each other and with the local environment.[43,44] The main difference between these brushes and binary brushes is that the phase domain structure is usually well ordered and periodic, allowing them to be useful in applications of nanopatterning and templates.[45,46]

One type of brush that is receiving intense attention consists of an architecture in which one block serves as a backbone filled with initiators (macromonomer) from which other polymer chains can be attached to[47] via a "grafting-through" process.[48] These are known in the literature as comb-graft copolymers. The vast majority of research dealing with these molecules has been in solution where they adopt a cylindrical configuration, and thus they are labeled as bottle brushes or cylindrical brushes. The interest here in taking this a step further and developing complex macromolecular architectures *within* grafted brush layers is related to the potential of controlled vertical gradients in brush composition and branching and thus forward logic for nanomechanical design. Moreover, by using a macromonomer approach, we can achieve not only extremely high branching density but also selective branching. Selective branching here implies attachment only at the top of the main backbone chain (not its entire length as in a cylindrical brush), leading to a brush-*block*-coil copolymer.[49] This can lead to uniquely enhanced backbone strengthening due to steric crowding, increased intramolecular interactions, and tailor-made chemical incompatibility between polymer segments.[50] Not until very recently have such complex brushes been able to be grown from the surface of silicon substrates as a result of advancements in polymerization methods such as ATRP and the breakthrough RAFT polymerization technique.[51,52] Furthermore, dense, uniform grafted brush layers consisting of these molecules have yet to be reported in the literature. Luzinov et al. have grafted binary brushes to a PGMA layer that serves as a "carpet" of functional epoxy grafting sites.[53] However, this is an extremely thin layer (monolayer, 1.5 nm thick) with a lack of physical properties and response mechanism. Sheiko et al. have established methods to graft side chains to a macroinitiator backbone with a gradient in spacing intervals along the backbone.[54] The authors are not concerned with fabricating grafted layers of these molecules because they just deposit individual molecules on the surface and observe their structure.[55,56]

Our aim is to build on this approach by fabricating novel polymer architectures in which one block is some environmentally responsive polymer (strong response to thermal or pH fluctuations) that is capped with a macroinitiator (macromonomer) in which other polymer chains can be grown from or attached to. However, the intention here is to have a very asymmetrical backbone in terms of the length of the surface block (very long) and the macroinitiator block (very short), which will result in a "palm-tree-like" polymer (Figure 1). The main points we address in this article are (1) the synthesis of vertically segregated brush layers using facile UV-initiated polymerization; (2) the characterization of the morphology at each synthesis step and the overall morphology of the complex layer; and (3) the design of a vertically graded nanomechanical response, which can be tuned by external temperature. With the palm-tree-like configuration, it is anticipated that because of the relatively high chain density at the top of the layer, a multilayer-type structure can result with varying degrees of vertical gradient.

Experimental Section

Materials. *N*,*N*-(Diethylamino)dithiocarbamoylbenzyl(trimethoxy)silane (SBDC) was synthesized according to a well-known proce-

---

(22) Bliznyuk, V. N.; Everson, M. P.; Tsukruk, V. V. *J. Tribol.* **1998**, *120*, 489. Tsukruk, V. V.; Bliznyuk, V. N. *Langmuir* **1998**, *14*, 446. Sidorenko, A.; Houphouet-Boigny, C.; Villavicencio, O.; McGrath, D. V.; Tsukruk, V. V. *Thin Solid Films* **2002**, *410*, 147. Ahn, H.; Julthongpiput, D.; Kim, D. I.; Tsukruk, V. V. *Wear* **2003**, *255*, 801. Tsukruk, V. V.; Sidorenko, A.; Yang, H. *Polymer* **2002**, *43*, 1695. Sidorenko, A.; Julthongpiput, D.; Luzinov, I.; Tsukruk, V. V. *Tribol. Lett.* **2002**, *12*, 101.

(23) Ito, Y.; Ochiai, Y.; Park, Y. S.; Imanishi, Y. *J. Am. Chem. Soc.* **1997**, *119*, 1619.

(24) Galaev, I.; Mattiasson, B. *Trends Biotechnol.* **1999**, *17*, 335.

(25) Jones, D. M.; Smith, R. R.; Huck, W. T. S.; Alexander, C. *Adv. Mater.* **2002**, *14*, 1130.

(26) Aksay, I. A.; Trau, M.; Manne, S.; Honma, I.; Yao, N.; Zhou, L.; Fenter, P.; Eisenberger, P. M.; Gruner, S. M. *Science* **1996**, *273*, 892.

(27) Dean, D.; Seog, J.; Ortiz, C.; Grodzinsky, A. J. *Langmuir* **2003**, *19*, 5526.

(28) Rixman, M. A.; Dean, D.; Ortiz, C. *Langmuir* **2003**, *19*, 9357.

(29) Qin, S. H.; Oin, D. Q.; Ford, W. T.; Resasco, D. E.; Herrera, J. E. *J. Am. Chem. Soc.* **2004**, *126*, 170.

(30) Gomez, F. J.; Chen, R. J.; Wang, D. W.; Waymouth, R. M.; Dai, H. J. *Chem. Commun.* **2003**, *2*, 190.

(31) Viswanathan, G.; Chakrapani, N.; Yang, H. C.; Wei, B. Q.; Chung, H. S.; Cho, K. W.; Ryu, C. Y.; Ajayan, P. M. *J. Am. Chem. Soc.* **2003**, *125*, 9258.

(32) Artyukhin, A. B.; Bakajin, O.; Stroeve, P.; Noy, A. *Langmuir* **2004**, *20*, 1442.

(33) Murat, M.; Grest, G. S. *Phys. Rev. Lett.* **1989**, *63*, 1074.

(34) Alexander, S. J. *J. Phys.* **1977**, *38*, 977.

(35) de Gennes, P. G. *Macromolecules* **1980**, *13*, 1069.

(36) Karim, A.; Tsukruk, V. V.; Douglas, J. F.; Satija, S. K.; Fetters, L. J.; Reneker, D. H.; Foster, M. D. *J. Phys. II* **1995**, *5*, 1441. Tsukruk, V. V. *Prog. Polym. Sci.* **1997**, *22*, 247. Tsukruk, V. V. *Adv. Mater.* **1998**, *10*, 253.

(37) Zhao, B.; Brittain, W. J. *J. Am. Chem. Soc.* **1999**, *121*, 3557. Zhao, B.; Brittain, W. J.; Zhou, W. S.; Cheng, S. Z. D. *J. Am. Chem. Soc.* **2000**, *122*, 2407. Sedjo, R.; Mirous, B. K.; Brittain, W. J. *Macromolecules* **2000**, *33*, 1492.

(38) Wittmer, J.; Johner, A.; Joanny, J. F. *Colloids Surf., A* **1994**, *86*, 85.

(39) Woodcock, S. A.; Chen, C.; Chen, Z. *Langmuir* **2004**, *20*, 1928.

(40) Gunari, N.; Schmidt, M.; Janshoff, A. *Macromolecules* **2006**, *39*, 2219.

(41) Zhang, Q.; Archer, L. A. *Langmuir* **2006**, *22*, 717.

(42) *Responsive Polymer Materials: Design and Applications*; Minko, S., Ed.; Blackwell Publishing: Ames, IA, 2006.

(43) Krausch, G.; Magerle, R. G. *Adv. Mater.* **2002**, *14*, 1579.

(44) Zhulina, E. B.; Birshtein, T. M.; Priamitsyn, V. A.; Klushin, L. I. *Macromolecules* **1995**, *28*, 8612.

(45) Park, M.; Christopher H.; Chaikin, P. M.; Register, R. A.; Adamson, D. H. *Science* **1997**, *276*, 1401.

(46) Sidorenko, A.; Tokarev, I.; Minko, S.; Stamm, M. *J. Am. Chem. Soc.* **2003**, *125*, 12211.

(47) Sheiko, S. S.; Möller, M. *Chem. Rev.* **2001**, *101*, 4099.

(48) Wintermantel, M.; Gerle, M.; Fischer, K.; Schmidt, M.; Wataoka, I.; Urakawa, H.; Kajiwara, K.; Tsukahara, Y. *Macromolecules* **1996**, *29*, 978.

(49) Neiser, M. W.; Muth, S.; Kolb, U.; Harris, J. R.; Okuda, J.; Schmidt, M. *Angew. Chem., Int. Ed.* **2004**, *43*, 3192.

(50) Rathgeber, S.; Pakula, T.; Wilk, A.; Matyjaszewski, K.; Beers, K. L. *J. Chem. Phys.* **2005**, *122*, 124904.

(51) McCormick, C. L.; Lowe, A. B. *Acc. Chem. Res.* **2004**, *37*, 312.

(52) Edmonson, S.; Osborne, V.; Huck, W. T. S. *Chem. Soc. Rev.* **2004**, *33*, 14−22.

(53) Iyer, K. S.; Zdyrko, B.; Malz, H.; Pionteck, J.; Luzinov, I. *Macromolecules* **2003**, *36*, 6519.

(54) Borner, H. G.; Duran, D.; Matyjaszewski, K.; da Silva, M.; Sheiko, S. S. *Macromolecules* **2002**, *35*, 3387.

(55) Lord, S. J.; Sheiko, S. S.; LaRue, I.; Lee, H.; Matyjaszewski, K. *Macromolecules* **2004**, *37*, 4235.

(56) Borner, H. G.; Beers, K.; Matyjaszewski, K.; Sheiko, S.; Moller, M. *Macromolecules* **2001**, *34*, 4375.

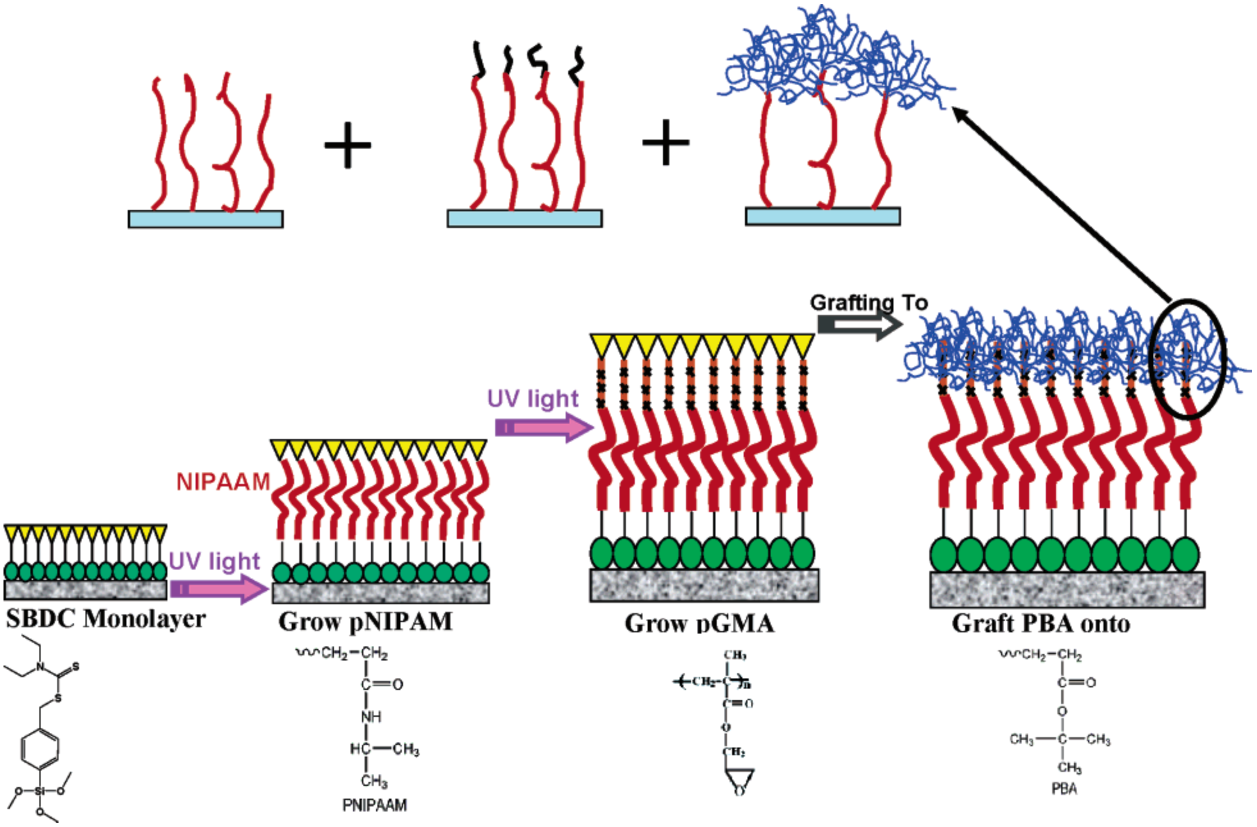

Figure 1. Schematic representation showing the overall layer construction and chemical structures starting with the SBDC monolayer, UV-initiated polymerization of pNIPAAM, UV-initiated polymerization of pGMA, and grafting of the COOH-PBA topmost layer.

dure[57] and was then distilled. Monomers *N*-isopropylacrylamide (NIPAAM) and glycidyl methacrylate (GMA) were purchased from Aldrich (Milwaukee, WI) and were >99% pure. NIPAAM was recrystallized from hexane and vacuum dried for 24 h. GMA was purified and stored in a sealed vial under argon at −15 °C. Carboxyl acid-terminated poly(butyl acrylate) (M_n: PBA = 42 500 g/mol with $M_w/M_n = 1.06$) was obtained from Polymer Source, Inc. Anhydrous toluene and DMF were obtained from Aldrich, further dried with sodium, and stored in a nitrogen-filled glovebox with a relative humidity not exceeding 2%. All other solvents were used as received. The silicon wafer {100} substrates were first cleaned in an ultrasonic bath for 30 min, placed in a hot (90 °C) bath (3:1 concentrated sulfuric acid/30% hydrogen peroxide) for 1 h, and then rinsed with Nanopure water (18 MΩ cm, Nanopure).

Layer Fabrication. An overall schematic of multistep layer fabrication is presented in Figure 1. The freshly cleaned silicon wafers were submerged in 4% toluene solutions of SBDC inside a nitrogen glovebox (RH < 1%) for 2 h to form the UV-initiating self-assembled monolayer (SAM). The wafers were transferred to individual custom-made rectangular quartz test tubes. NIPAAM (10% in water) was transferred to the sealed test tube by syringe, and the solution with the wafer was further bubbled with argon for at least 1 h. In the next step, NIPAAM was polymerized at room temperature by exposing the tube to UV irradiation at 5 mW/cm^2. This was found to be optimal because higher power resulted in immediate cross linking and gelation of the solution whereas lower power resulted in extremely slow or completely suppressed growth. The growth rate was found to be roughly 10 nm/h as verified by a series of ellipsometry and atomic force microscopy (AFM) measurements. After polymerization, the pNIPAAM layer was rinsed three times in ethanol, sonicated for 30 min in ethanol, and rinsed three more times. In the next step, the wafer was put into a fresh test tube and sealed, and GMA (10% in DMF) was added by syringe. Polymerization took place after UV exposure of 3 mW/cm^2 for 1 h, which corresponded to 1 to 2 nm of pGMA as verified by ellipsometry and AFM. Afterward, the sample was cleaned as in the previous step, except with DMF in this case. Finally, the PBA layer was added via a grafting-to process with the available epoxy groups in pGMA. The PBA solutions were prepared in DMF at 5.0 wt % polymer and spin coated onto the brush-modified silicon wafers at 3000 rpm. The samples were then annealed to facilitate grafting between the epoxy and carboxyl acid groups[58] and rinsed and sonicated in the same fashion as described above with DMF.

Characterization. All thickness measurements were obtained with a COMPEL automatic ellipsometer (InOm Tech, Inc.) with an incident angle of 70°.[59] The contact angle was measured with a sessile drop method using 2 μL droplets of Nanopure water, which were captured with a custom-built digital microscope. XPS was done with a Perkin-Elmer Multitechnique Chamber (model 5500). The etching rate was measured to be 1 nm/min measured against SiO$_2$. AFM (MultiMode and Dimension 3000, Veeco Metrology) was used for topographical and phase imaging in air according to the procedures adapted in our laboratory.[60,61] Unless otherwise noted, all AFM images were obtained using the light tapping regime governed by the setpoint ratio (rsp), which is defined as the ratio of the operating setpoint (amplitude) to the free oscillating amplitude of the cantilever. The attractive regime, or light tapping, is characterized by an rsp of 0.9−1, and the repulsive regime, or hard tapping, has an rsp of 0.4−0.7. AFM tips were MikroMasch (Talin, Estonia) V-shaped contact tips with a nominal spring constant ranging from 1 to 6 N/m. We used softer contact tips in the noncontact regime in order to get suitable scans of the soft NIPAAM surface at room temperature. The tips had a radius of less than 30 nm, which

---

[57] de Boer, B.; Simon, H. K.; Werts, M. P. L.; van der Vegte, E. W.; Hadziioannou, G. *Macromolecules* **2000**, *33*, 349.

[58] Fisch, W.; Hofmann, W. *Macromol. Chem. Phys.* **1961**, *44*−*46*, 8.

[59] Motschmann, H.; Stamm, M.; Toprakcioglu, C. *Macromolecules* **1991**, *24*, 3681.

[60] Ratner, B., Tsukruk, V. V., Eds. *Scanning Probe Microscopy of Polymers*; ACS Symposium Series; American Chemical Society: Washington, DC, 1998; Vol. 694.

[61] Tsukruk, V. V. *Rubber Chem. Technol.* **1997**, *70*, 430.

was determined by scanning a gold nanoparticle reference sample.[62] AFM scratch tests at each temperature were conducted with a sharp needle. After the scan of the scratched area was obtained, the average thickness in the fluid was obtained over a 10 × 10 μm^2 area with a height histogram distribution. Despite that, this procedure could potentially lead to some underestimation of the film thickness because of the layer compression; this effect is usually insignificant under the light tapping conditions used in this work. In fact, as has been demonstrated for a number of grafted polymeric layers by direct comparison of scratch tests and independent measurements (e.g., see refs 61, 65, and 67), this approach gives very consistent results if conducted correctly with possible underestimations well below 10%.

Force volume mode, which utilizes the collection of the AFM force distance curves (FDC) over selected surface areas, was used for nanomechanical analysis of the brush layers. A single FDC obtains the forces acting on the tip as it approaches and retracts from a point on the sample surface.[63] Obtaining arrays of FDCs allows for the micromapping of the mechanical properties of polymer surfaces with nanometer-scale resolution while obtaining topographical information simultaneously.[64,65] Typically, we collected 16 × 16 arrays over a 2 × 2 μm^2 surface areas to do micromapping. Data collected were processed using an MMA software package developed in our laboratory that provides the means of calculation of the localized elastic modulus.[66] The loading curves, the elastic modulus, reduced adhesive forces, and surface histograms of elastic moduli and adhesive forces were obtained from experimental images as described elsewhere on many occasions.[66,67] Briefly, we used a modified Hertzian model to fit the experimental loading curves and derive the elastic modulus. During experiments, all precautions were taken to avoid plastic deformation by keeping a low threshold and minimum penetration and testing the surface morphology after force volume measurements to control any presence of indentation marks. In the case of large indentations, as we demonstrated earlier, Sneddon's model can be applied instead of the Hertzian model that can modify the numerical values by 15%. In all cases, surface force studies in Nanopure water did not detect any significant long-range repulsive forces, but instead a clear jump-in phenomenon was observed that indicated the contact point used in the data analysis. Spring constants of cantilevers were determined from the resonance frequencies and the tip-on-tip method according to the procedures described earlier.[68,69] The tips used for MMA probing were silicon nitride with a radius of 60−90 nm and a spring constant ranging from 0.1 to 0.8 N/m.

Switching of the Brushes. The brushes were switched to drive the strong collapse/swelling of the NIPAAM sublayer above and below the LCST (32°). The brushes had to be placed in a fluid environment (water) to drive this phase transition. The samples were placed on a Peltier heating/cooling stage (Melcor Co.) that was heated to the desired temperature via an interfaced thermal controller (ILX Lightwave) with a resolution of 0.001 °C and a stability of ±0.005 °C over 24 h. The fluid (water) was injected into the system by taking advantage of capillary forces between the AFM tip and sample. After adding water, the system was allowed 2 h to reach equilibrium after the temperature change.

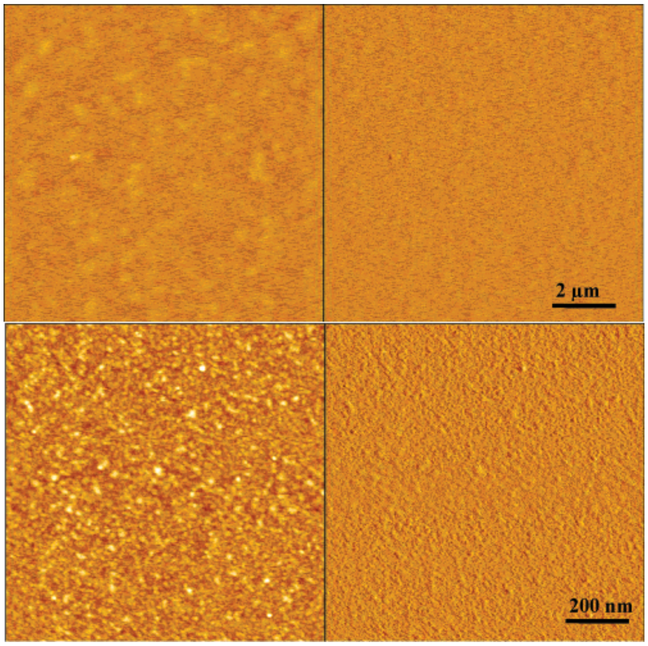

Figure 2. AFM tapping mode images (topography, left; phase, right) of the SBDC monolayer at 10 × 10 μm^2 (top) and 1 × 1 μm^2 (bottom). The *z* scale is 5 nm.

Results and Discussion

Study of Layer Growth. The foundation of the branched hierarchal polymer brush is the stable formation of the SBDC monolayer, which is the UV-initiating SAM (Figure 1). It should be noted here that this initiator is advantageous for a few reasons, the main reason being that is nonreactive with nearly all vinyl monomers.[70] Furthermore, the "living" nature of the dithiocarbamyl radical has been well documented and shown to be reversible,[71] allowing easy reinitiation for the polymerization of different monomers, making it ideal to use in these complex multicomponent brushes. Most importantly, this photoiniferter technique leads to the ability to conduct RAFT polymerization at room temperature without the need for an elaborate setup.

The monolayer was optimized with several iterations of coating parameters (concentration and assembly time). Once the reaction was terminated with rinsing, the wafers were either kept in solution and protected from light or immediately scanned with AFM. AFM images of the SBDC monolayer reveal highly uniform and clean layer formation on a large scale, with the surface rms roughness measured over a 1 × 1 μm^2 area of 0.2 nm (Figure 2). Concurrently obtained phase images presented here for this surface (Figure 2) and below for other grafted layers display uniform chemical composition of the surface studied here without any significant variations in the phase signal that can be associated with phase separation or gelation or other occurrences of nonuniformity in the topmost surface layers.

Theoretical estimates of SBDC SAM thickness for an ideal close-packed monolayer is about 1.4 nm.[72] This thickness was confirmed with ellipsometry, which along with very smooth surface morphology indicated the formation of a uniform SAM with the upright orientation of molecules (Table 1). The ellipsometry thickness of the SBDC SAM layer is similar to

---

[62] Radmacher, M.; Tilmann, R. W.; Gaub, H. E. *Biophys. J.* **1993**, *64*, 735.

[63] Cappella, B.; Dietler, G. *Surf. Sci. Rep.* **1999**, *34*, 1.

[64] *Advances in Scanning Probe Microscopy of Polymers*; Tsukruk, V. V., Spencer, N. D., Eds.; Macromolecular Symposia, 2001, Vol. 167.

[65] *Microstructure and Microtribology of Polymer Surfaces*; Tsukruk, V. V., Wahl, K., Eds.; American Chemical Society: Washington, DC, 1999; Vol. 741.

[66] Tsukruk, V. V.; Gorbunov, V. V. *Probe Microsc.* **2002**, *3*−*4*, 241. Huang, Z.; Chizhik, S. A.; Gorbunov, V. V. *J. Mater. Sci.* **1998**, *33*, 4905. Tsukruk, V. V.; Huang, Z. *Polymer* **2000**, *41*, 5541.

[67] Kovalev, A.; Shulha, H.; LeMieux, M. C.; Myshkin, N.; Tsukruk V. V. *J. Mater. Res.* **2004**, *19*, 716. Shulha, H.; Kovalev, A.; Myshkin, N.; Tsukruk, V. V. *Eur. Polym. J.* **2004**, *40*, 949.

[68] Hazel, J. L.; Tsukruk, V. V. *Thin Solid Films* **1999**, *339*, 249.

[69] Hazel, J. L.; Tsukruk, V. V. *J. Tribol.* **1998**, *120*, 814.

[70] de Boer, B.; Simon, H. K.; Werts, M. P. L.; van der Vegte, E. W.; Hadziioannou, G. *Macromolecules* **2000**, *33*, 349.

[71] Otsu, T.; Matsunaga, T.; Doi, T.; Matsumoto, A. *Eur. Polym. J.* **1995**, *31*, 67.

[72] Rahane, S. B.; Kilbey, S. M.; Metters, A. T. *Macromolecules* **2005**, *38*, 8202.

Table 1. Characteristics of the Surface Layers

layer	thickness (nm)	microroughness (nm)	contact angle (deg)	elastic modulus (MPa)
SBDC SAM	1.4	0.2	60	NA
pNIPAAM	19	0.9	70	NA
pGMA	2	0.3	54	NA
PBA-COOH	5	0.6	75	NA
total film				
dry state	25	0.6	NA	60
water, 10 °C	34	1.8		15
water, 50 °C	17	1.3		45

previously observed SBDC SAM thicknesses.[1,73,74] The calculated SBDC initiator density was 2.6 molecules/nm^2. This surface-tethered initiator density is consistent with literature data on SAM surface densities reported for controlled polymerizations.[75] The continued growth of the polymer layer when the sample is again irradiated witih UV light after an interruption that proved the living character of surface-initiated photopolymerization is given in the literature.[57]

At a UV light intensity of 5 mW/cm^2, an optimal layer growth of roughly 10 nm/h was achieved. The process used here was more empirical—a suitable medium between gelation and reasonable layer growth that was monitored at each iteration with ellipsometry. Higher intensities resulted in quick gelation in the system due to excessive cross linking between side chains or formations in the bulk solution. However, lower intensities resulted in extremely slow, nonuniform growth. The kinetics involving the polymerization on a silicon surface from this iniferter monolayer is beyond the scope of this article and has already been studied.[70] It was instrumental to keep the initial pNIPAAM layer to around 20 nm in order to observe a vertical gradient.

In fact, the literature data have shown that under these particular conditions the grafting density for dimethylacryl amide (PDMAAm) should be one chain per 20−30 nm^2. This value is lower than values obtained for another surface-initiated polymerizations (1 polymer chain per 2−9 nm^2)[76−79] because of very low initiator efficiency (0.065).[74] Kinetic studies of surface-initiated photopolymerization revealed that a light intensity of 5 mW/cm^2 is optimal for the linear growth of polymer chains from the surface.[57,73,80] It is worth noting that at this intensity no cross linking has been observed, as can be concluded from the preservation of intact swelling−collapse behavior of the pNIPAAM chains as will be demonstrated below.

The presence of pNIPAAM was verified with ellipsometry measurements, AFM, and XPS (below). The pNIPAAM dry thickness of all samples was within 19 ± 1 nm (Table 1). The dry-state AFM images reveal fine, contamination-free morphology with a surface rms roughness around 1 nm (Figure 3). In addition, the light tapping regime during scanning was necessary to avoid instabilities while scanning the extremely soft pNIPAAM below LCST, which is another characteristic proving the presence of a strongly attached pNIPAAM layer.[81]

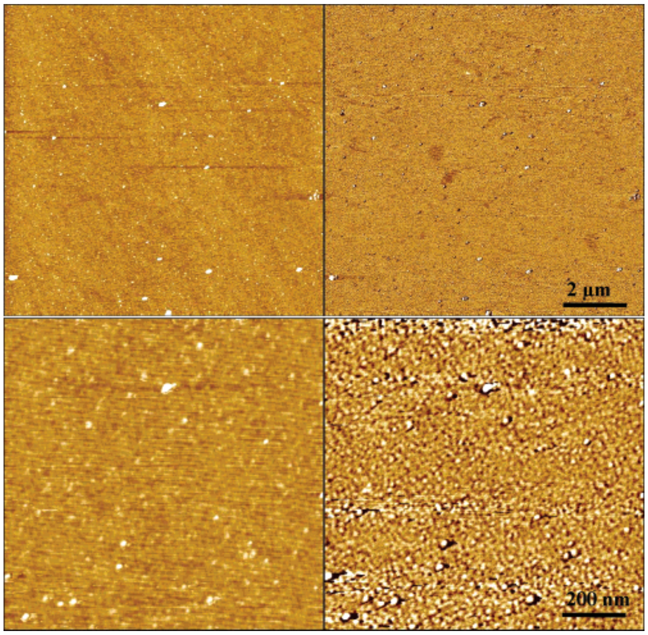

Figure 3. AFM tapping mode images (topography, left; phase, right) at room temperature of the as-grown first grafted layer (NIPAAM) by UV-RAFT polymerization. The top is 10 × 10 μm^2, and the bottom is 1 × 1 μm^2. The z scale is 5 nm.

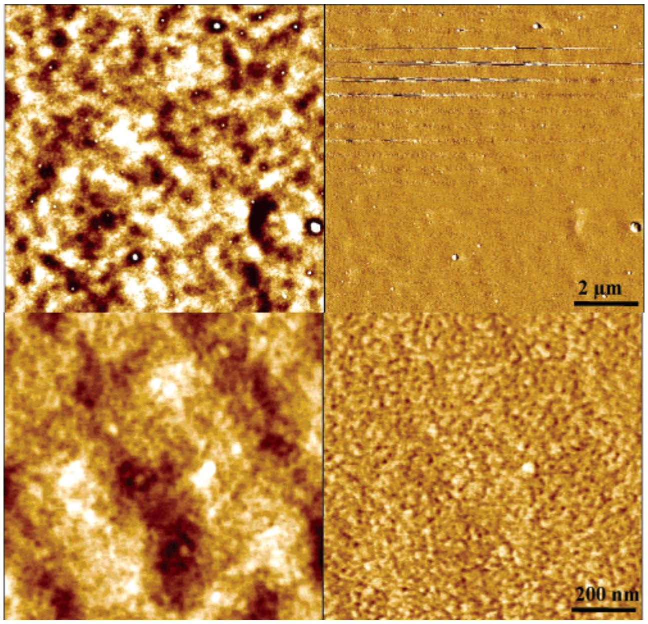

Figure 4. AFM tapping mode images (topography, left; phase, right) at room temperature of a pGMA macromonomer. The top is 10 × 10 μm^2, and the bottom is 1 × 1 μm^2. The z scale is 5 nm.

The next step was the deposition of GMA to act as a macroinitiator (Figure 1). Polymerization was carried out below the pNIPAAM LCST to keep the chains swollen in the solvent, making them more accessible to the GMA monomer. Figure 4 represents the brush after copolymerization of the GMA macroinitiator with pNIPAAM. As can be seen, although the surfaces remain relatively smooth on a large scale (rms roughness is 1.2 nm), the morphology changes significantly from that of the pure pNIPAAM layer. In addition, the contact angle dropped from 70° for the pure pNIPAAM layer to 54° with the addition of pGMA. A thickness of 2 ± 0.5 nm indicated that each pGMA chain attached to a pNIPAAM has six to seven grafting sites available for incoming polymer in the subsequent grafting-to stage to complete the topmost layer (Figure 1). This estimation has been obtained from the number of grafting sites estimated for pGMA chains (not exceeding 2−3 per chain) and the overall

---

[73] Rahane, S. B.; Kilbey II, S. M.; Metters, A. T. *Macromolecules* **2005**, *38*, 8202.

[74] Harris, B. P.; Metters, A. T. *Macromolecules* **2006**, *39*, 2764.

[75] Gopireddy, D.; Husson, S. M. *Macromolecules* **2002**, *35*, 4218.

[76] Schmidt, R.; Zhao, T.; Green, J.-B.; Dyer, D. J. *Langmuir* **2002**, *18* 1281.

[77] Jordan, R.; Ulman, A.; Kang, J. F.; Rafailovich, M. H.; Sokolov, J. *J. Am. Chem. Soc.* **1999**, *121*, 1016.

[78] Prucker, O.; Rühe, J. *Macromolecules* **1998**, *31*, 602.

[79] Zhao, B.; Brittain, W. J. *Macromolecules* **2000**, *33*, 342.

[80] Kidoaki, S.; Ohya, S.; Nakayama, Y.; Matsuda, T. *Langmuir* **2001**, *17*, 2402.

[81] Harmon, M. E.; Kuckling, D.; Frank, C. W. *Langmuir* **2003**, *19*, 10660.

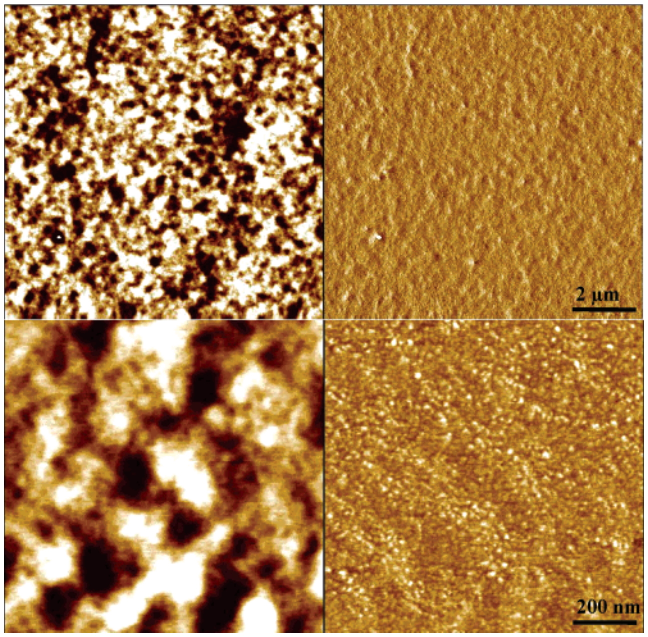

Figure 5. AFM tapping mode images (topography, left; phase, right) at room temperature of the topmost grafted layer, COOH-PBA. The top is 10 × 10 μm^2, and the bottom is 1 × 1 μm^2. The *z* scale is 5 nm.

molecular weight of the chains according to the known approach.[82] Thus, an important aspect of these complex brushes realized by grafting onto a macroinitiator is that by incorporating a 2-nm-thick grafting interlayer the availability of grafting sites is comparable to anchoring epoxy-terminated SAMS on a silicon oxide surface.[83,84]

The final fabrication step was to attach PBA to the available grafting sites (Figure 1). When preformed COOH-terminated PBA polymer was grafted to the pGMA macromonomer, the measured thickness was 5 ± 1 nm (Table 1). This value is higher than the 3 nm typical for this molecular weight PBA via grafting to epoxy-terminated SAMs.[85,86] An indication of having high neighboring chain interaction and potentially significant entropic effects is to be in the polymer brush regime in which the interchain distance is substantially less than the radius of gyration of the corresponding free polymer chain.[35] For the PBA used here, the radius of gyration has been calculated to be 2.2 nm.[76] Thus, the grafting distance was less than the radius of gyration of these PBA chains, indicating that the chains are indeed in a stretched, brushlike conformation. AFM images of the final topmost PBA layer shown in Figure 5 demonstrate a clean, homogeneous surface with a microroughness not exceeding 1.5 nm, indicating extremely homogeneous, uniform grafting.

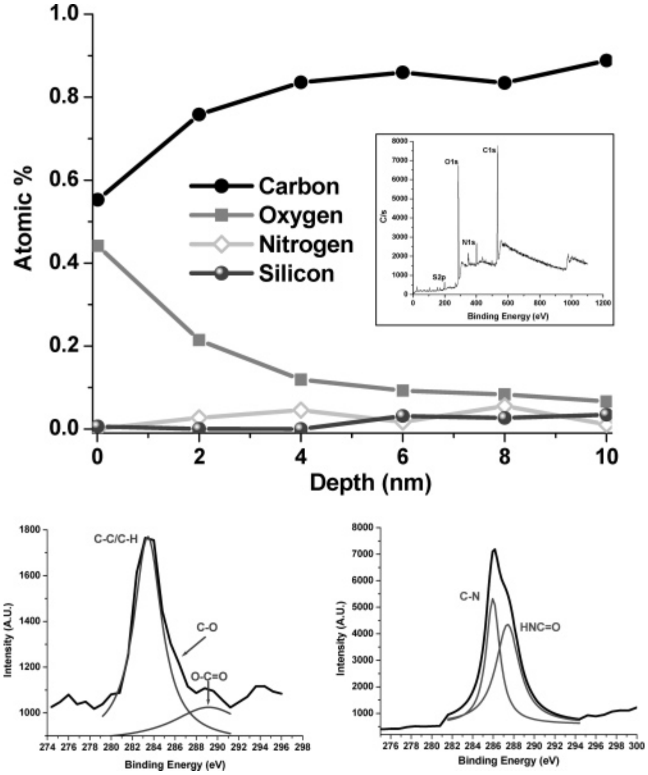

Figure 6. XPS data on the overall branched polymer brush layer. At the top are depth-profiling results over the probing of the first 10 nm of the layer, which is deep enough to probe all layers in this brush. The inset is the overall survey scan showing characteristic peaks. At bottom are the extracted data showing bands of specific groups for the polymers making up the grafted brush layer.

This data monitored at each grafting step clearly shows that a complex, multicomponent, multilayered, branched brush can be constructed using grafting-from and grafting-to processes in series and that the overall dry thickness was around 25 nm (Figure 1, Table 1). To confirm the vertical distribution of different layers, we conducted XPS surveys taken to allow for depth profiling of the brush layer (Figure 6). At a rate of 1 nm/min, a signature from the full top two layers should be observed, as well as that from a fraction of the pNIPAAM bottom layer (Figure 6). This variation corresponds to the overall drop in oxygen concentration because the ratio of oxygen in pNIPAAM is much lower as compared with those in PBA and pGMA. The peak at 289 eV is a clear indication of the O−C═O bond in PBA and GMA, along with the shoulder at 286 eV (Figure 6).[87,88] The peak at 285.8 eV can be assigned to the C−N bond, and HNC═O is represented at 287.4 eV.[89] The sulfur peak represents residual initiator remaining from the SBDC. Therefore, XPS along with previously discussed AFM and ellipsometry results confirmed the layered composition of the fabricated polymer films.

LCST Transition within Grafted Film. After layer fabrication, it was imperative to test the LCST phase behavior of pNIPAAM confined within the layered structure. It is well known that pNIPAAM undergoes a strong response to temperature around 32 °C, and our hypothesis here is that this collapse/swelling will change the overall vertical layering, leading to a distinct variation of the elastic response. To monitor this, we measured the thickness of the overall layer above and below the LCST with in-situ AFM scratch tests. Initial AFM scratch tests done in air at 50 and 10 °C showed no change in thickness. In fact, several recent reports claim that pNIPAAM layers respond strongly only if they are also in a favorable solvent (such as water) and that the transition is not apparent under ambient

---

(82) Luzinov, I.; Julthongpiput, D.; Malz, H.; Pionteck, J.; Tsukruk, V. V. *Macromolecules* **2000**, *33*, 1043.

(83) Luzinov, I.; Julthongpiput, D.; Tsukruk, V. V. *Polymer* **2001**, *42*, 2267.

(84) Tsukruk, V. V.; Luzinov, I.; Julthongpiput, D. *Langmuir* **1999**, *15*, 3029. Luzinov, I.; Julthongpiput, D.; Liebmann-Vinson, A.; Cregger, T.; D. Foster, M.; Tsukruk, V. V. *Langmuir* **2000**, *16*, 504.

(85) Julthongpiput, D.; LeMieux, M. C.; Tsukruk, V. V. *Polymer* **2003**, *44*, 4557.

(86) LeMieux, M. C.; Julthongpiput, D.; Bergman, K. N.; Cuong, P. D.; Ahn, H.-S.; Lin, Y.-H.; Tsukruk, V. V. *Langmuir* **2004**, *20*, 10046.

(87) Matrab, T.; Chehimi, M. M.; Perruchot, C.; Adenier, A.; Guillez, A.; Save, M.; Charleux, B.; Cabet-Deliry, E.; Pinson, J. *Langmuir* **2005**, *21*, 4686.

(88) Zhang, Y.; Tan, K. L.; Liaw, B. Y.; Liaw, D. J.; Kang, E. T. *Thin Solid Films* **2000**, *374*, 70.

(89) Ying, L.; Kang, E. T.; Neoh, K. G. *Langmuir* **2002**, *18*, 6416.

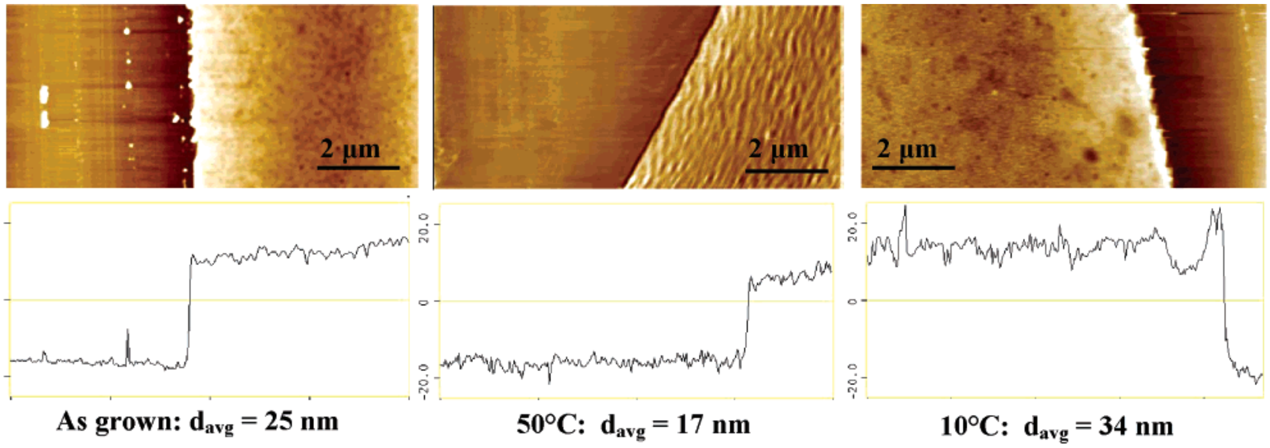

As grown: $d_{avg} = 25$ nm **50°C:** $d_{avg} = 17$ nm **10°C:** $d_{avg} = 34$ nm

Figure 7. AFM analysis of scratch tests of the overall layer done in water at different temperatures compared with the as-grown dry-state condition (left). As can be seen, the layer undergoes dramatic changes in thickness on going from 50 °C (middle) to 10 °C (right) as well as noticeable changes in overall layer morphology.

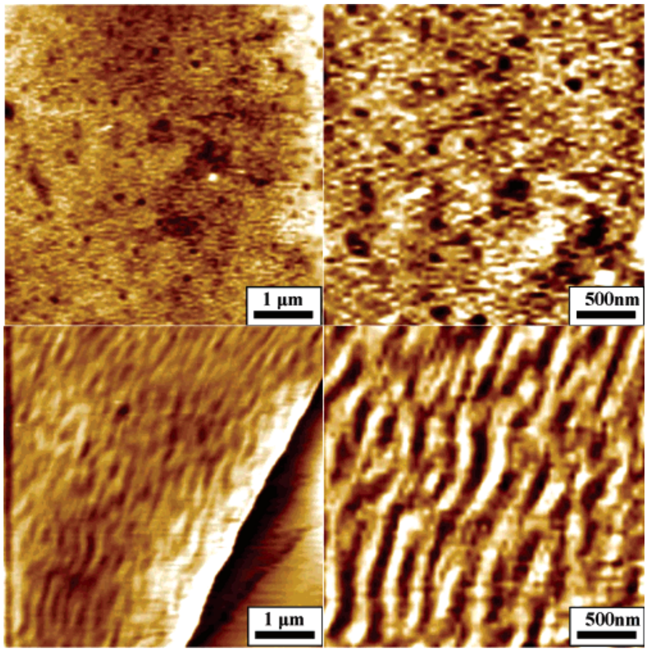

Figure 8. AFM tapping mode topography images in water of the overall brush at different temperatures. The top row is the brush layer at 10 °C, and the bottom row is at 50 °C.

conditions.[90,91] Indeed, the same measurements in water revealed significant changes (Figure 7). The layer reached an overall thickness of around 34 nm at 10 °C, and the layer thickness collapsed to 17 nm above the LCST (Figure 7, Table 1).

Along with this change in thickness, there is a marked change in the morphology of the topmost PBA layer at different temperatures with the appearance of a long, wavy surface at 50 °C (Figure 8). Such a change can result only from variations in the underlying pNIPAAM layer because separate studies of the PBA surface at these different temperatures resulted in no change in morphology. This is an important result revealing that at 10 °C, with a swollen underlying brush layer, the PBA chains adopt a random structure. However, at 50 °C, where the underlying layer strongly collapses above the LCST, reducing the overall thickness by 50%, the PBA top layer adopts a constrained morphology with distinct elongated cluster domains (Figure 8).

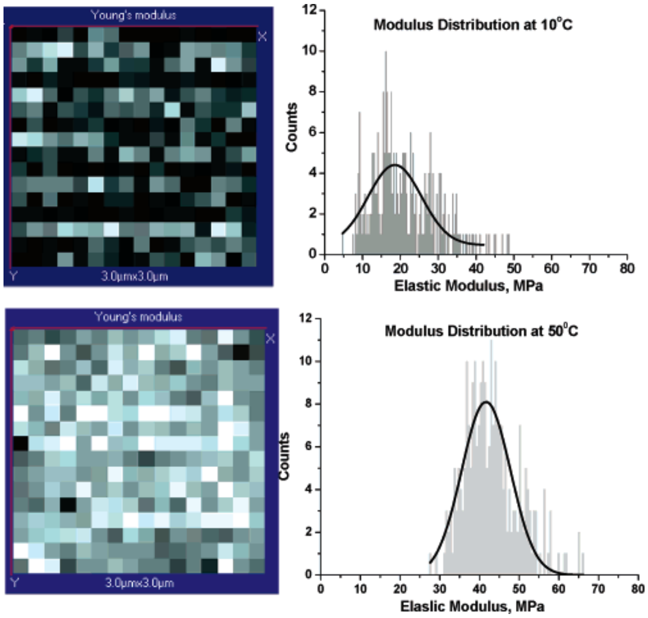

Figure 9. (Left column) Force−volume images with 16 × 16 resolution mapping of the overall layer elastic modulus over a 3 × 3 μm^2 area. Brighter areas correspond to higher modulus values. This mapping results from nanomechanical probing in water at 10 °C (top, modulus range is 0−50 MPa) and 50 °C (bottom, modulus range is 0−70 MPa). (Right column) Resulting surface modulus histograms from the corresponding modulus maps. The elastic modulus is the average value for each data point over the entire indentation range, and the data are fitted with a Lorentzian curve. The adhesive histograms are similar for both temperatures (not shown).

These types of changes should be sufficient to induce distinct density gradients within the layer and thus the overall nanomechanical properties, as were tested with MMA approach.

Temperature-Dependent Nanomechanical Properties. This MMA analysis can determine the modulus of the surface layers with nanoscale resolution directly in fluid at a specific temperature, at 10 °C (below the LCST) and at 50 °C (above the LCST) (Figure 9). The resulting surface histograms of the elastic modulus presented show a unimodal distribution of the elastic modulus that is expected for a surface with a homogeneous top phase. The average value is close to 15 MPa, which is lower than a modulus of 50−100 MPa for PBA in the collapsed state above $T_g = -5$ °C but due to averaging over entire penetration, is a lower value

---

(90) Kuckling, D.; Hoffmann, J.; Plötner, M.; Ferse, D.; Kretschmer, K.; Adler, H.-J. P.; Arndt, K.-F.; Reichelt. R. *Polymer* **2003**, *44*, 4455.

(91) Kim, S.; Healy, K. E. *Biomacromolecules* **2003**, *4*, 1214.

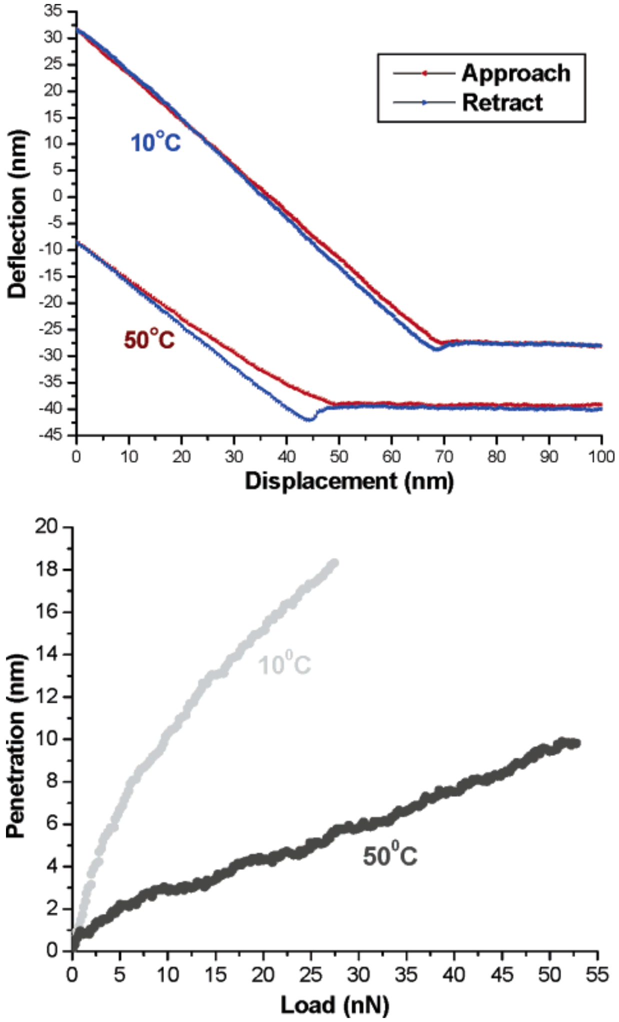

Figure 10. Typical force–distance curves (top) and resulting load–penetration curves (bottom) obtained in the nanomechanical analysis and averaged over 20+ individual curves with a standard deviation for each pixel below 10% at the indicated temperature in water.

due to pNIPAAM in a swollen state.[85,86] For a temperature above the LCST, the elastic modulus has a higher value around 45 MPa (Figure 9).

An examination of individual FDCs shows that the overall adhesion is very similar at both temperatures with a slightly higher adhesion for 50 °C, which is expected for a PBA top layer well above its glass-transition temperature (Figure 10). The overall slope of FDC at 10 °C is slightly lower over full penetration, which corresponds to a more compliant state as concluded from the elastic modulus histograms (Figure 9). Conversion of the FDCs into loading curves further confirms that a more compliant surface is associated with the 10 °C state (Figure 10). For 50 °C, the loading curve is virtually linear, indicating a uniform elastic compression for the penetration reaching 10 nm. However, below LCST (10 °C) the loading curve shows two distinct regions of different slopes implying the AFM tip is feeling nonuniform compliancy from the brush layer related to its stratification below the LCST. At this temperature, compliant behavior is observed for the initial 8–10 nm of deformation, followed by a much stiffer response (Figure 10).

Considering these results, we suggest the schematics of temperature-dependent vertical stratification in our surface film (Figure 11). First, we suggest that at elevated temperature above the LCST the central, temperature-sensitive pNIPAAM layer is in its collapse state, which results in a compact overall structure with two major layers forming the 17 nm film. The uniform elastic deformation with relatively high elastic modulus, 45 MPa, is caused by comparable elastic properties of PBS above the T_g (50–100 MPa) and pNIPAAM above the LCST (20–100 MPa).[77,83] Below the LCST when pNIPAAM chains become swollen in water, a completely different nanomechanical response is observed. Here, the initial elastic modulus is much lower because the overall deformation of the film under the AFM tip is controlled by the most compliant component, a highly swollen pNIPAAM layer with 30 nm thickness with an extremely low modulus around 1 MPa (Figure 11).[92] Only at very high deformation does the overall resistance of the PBA layer and the compressed pNIPAAM layer becomes more significant, with the elastic modulus increasing to 35 MPa. The overall behavior of the stratified polymer layer designed here is reminiscent of the nonlinear elastic response of trilayered surface film composed of a soft, rubbery block-copolymer layer sandwiched between a SAM and the photopolymerized acrylate topmost layer reported previously.[93] However, in those studies, the nonlinear elastic response is triggered by the local stresses but cannot be tuned by varying the external temperature. In contrast, the current design creates a stratified grafted layer with a completely reversible nanomechanical response that can be turned on and off on-demand by lowering and raising the temperature in the vicinity of the LCST point. Moreover, unlike previous designs (e.g., binary brushes) the reorganization of stratified layers does not significantly change the surface composition, preserving its overall hydrophobic character.

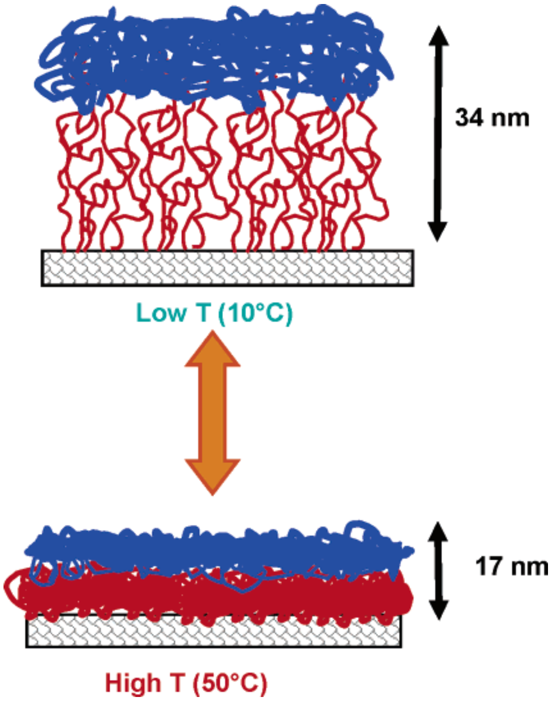

Figure 11. Schematic depicting the structural reorganization of the overall branched polymer brush in water at the two temperatures indicated above and below the LCST. Below the LCST, the pNIPAAM chains are highly swollen and PBA is collapsed (bad solvent conditions) whereas above the LCST, pNIPAAM is collapsed into tight clusters toward the substrate. As this occurs, because of the high density of PBA in the top layer, PBA is pulled into tighter clusters because it is still in a bad solvent (water), and NIPAAM collapses strongly (more than 100% as indicated by scratch tests in water).

---

[92] Harmon, M. E.; Kuckling, D.; Pareek, P.; Frank, C. W. *Langmuir* **2003**, *19*, 10947.

[93] Tsukruk, V. V.; Ahn, H.-S.; Sidorenko, A.; Kim, D. *Appl. Phys. Lett.* **2002**, *80*, 4825. Sidorenko A.; Ahn, H.-S.; Kim, D.-I.; Yang, H.; Tsukruk, V. V. *Wear* **2002**, *252*, 946.

These temperature-sensitive, adaptive polymer layers with the pNIPAAM layer “hidden” beneath the rubbery hydrophobic PBA topmost layer represent an interesting example of nanoscale engineering the surfaces with properties such as adhesion and elastic modulus and multilevel structural reorganization that are responsive to various fluidic and temperature fluctuations.

Acknowledgment. Funding from AFOSR (FA9550-05-1-0209) and the National Science Foundation (DMR-00308982) is gratefully acknowledged. We kindly thank Jim Anderegg for technical support with XPS measurements.

LA061723K